Journal of Applied Physics

Effect of multipole excitations in electron energy-loss spectroscopy of surface plasmon modes in silver nanowires

Cite as: J. Appl. Phys. **116**, 223101 (2014); https://doi.org/10.1063/1.4903535
Submitted: 08 October 2014 • Accepted: 19 November 2014 • Published Online: 08 December 2014

Xiuli Zhou, Anton Hörl, Andreas Trügler, et al.

View Online Export Citation CrossMark

ARTICLES YOU MAY BE INTERESTED IN

Investigation on the localized surface plasmon resonance (LSPR) of silver nanoparticles using electron energy loss spectroscopy (EELS) simulation
AIP Conference Proceedings **2023**, 020016 (2018); https://doi.org/10.1063/1.5064013

Electron energy-loss spectroscopy of surface plasmon activity in wrinkled gold structures
The Journal of Chemical Physics **153**, 224703 (2020); https://doi.org/10.1063/5.0031469

Enhanced semiconductor optical absorption via surface plasmon excitation in metal nanoparticles
Applied Physics Letters **86**, 063106 (2005); https://doi.org/10.1063/1.1855423

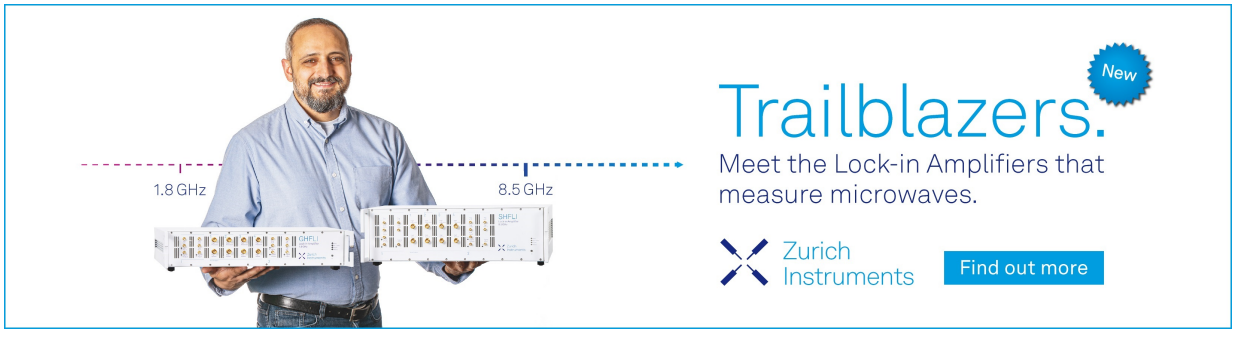

© 2014 AIP Publishing LLC.

AIP Publishing

Effect of multipole excitations in electron energy-loss spectroscopy of surface plasmon modes in silver nanowires

Xiuli Zhou,[1] Anton Hörl,[2] Andreas Trügler,[2] Ulrich Hohenester,[2] Theodore B. Norris,[1] and Andrew A. Herzing[3,a)]
[1]*Center for Ultrafast Optical Science, University of Michigan, Ann Arbor, Michigan 48109, USA*
[2]*Institut für Physk, Karl-Franzens-Universität Graz, 8010 Graz, Austria*
[3]*Material Measurement Laboratory, National Institute of Standards and Technology, Gaithersburg, Maryland 20899, USA*

(Received 8 October 2014; accepted 19 November 2014; published online 8 December 2014)

We have characterized the surface plasmon resonance (SPR) in silver nanowires using spatially resolved electron energy loss spectroscopy (EELS) in the scanning transmission electron microscope. Non-symmetric EELS spectra due to high-k SPR propagation along the nanowire and spectral shifts due to higher-order mode excitation are observed when the beam is positioned near the tip of the nanowire. When the beam is far from the tip region and on the side of nanowire, no spectral shifts are observed as the beam is scanned in the radial direction of the nanowire. The experimental spectra are compared with three different theoretical approaches: direct numerical calculation of the energy loss, analytical models for energy loss, and numerical simulations using an optical model. All three models reproduce the spectral shifts as the electron beam approaches the cap of the nanowire. The analytical model reveals the origin of the shifts in high-order plasmon mode excitation. © *2014 AIP Publishing LLC*. [http://dx.doi.org/10.1063/1.4903535]

I. INTRODUCTION

The surface plasmon resonance (SPR) modes of metal nanoparticles (NPs) enable the development of nano-optics and the manipulation of light at length scales far below the diffraction limit. In recent years, researchers have developed an extraordinary degree of control over the propagation of confined optical modes on the nanoscale in a variety of metallic systems. The character of SPR modes has been studied for varieties of geometries, including cubes,[1] prisms,[2] rods, and wires.[3–5] Metal nanowires are of particular interest since they may serve as the building blocks of more complex plasmonic systems or circuits. Metal nanowires exhibit an enhanced polarizability compared to more spherical shapes, and their resonance frequency can be tuned by changing their length and/or diameter and the composition of the surrounding medium. Some recently published theoretical analysis and experimental measurements have illustrated their optical properties and potential applications.[6–8]

In order to determine their spectral properties or their suitability for various applications, SPR modes are typically excited optically. In this case, it is difficult to study the spatial modes in great detail since no optical characterization with truly single-nanometer spatial resolution exists. However, electron energy loss spectroscopy (EELS) performed in the scanning transmission electron microscope (STEM) is capable of such resolution. In recent years, EELS has become a powerful tool to study optical-frequency SPR modes in individual nanostructures as a result of the improved energy resolution enabled by electron monochromators.[4,5,9] In this case, the attainable energy resolution approaches the width of SPR excitations in noble metals[10] and the signal can be acquired with nanometer-scale spatial resolution.[11]

Theoretical and experimental investigations of SPR excitation using EELS have been conducted on a variety of nanostructures, including single NPs of various shapes, nanoparticle arrays, thin films, and composite metamaterials.[10,12–16] Specifically for wire-type structures, Nicoletti *et al.*[17] and Rossouw *et al.*[18] have both recently utilized EELS to map the spatial extent of SPR's in single silver nanorods. They observed confined modes along the length of the wires as well as anti-node bunching of high-order resonant modes at the nanowire ends. They illustrated mode confinement effects and interpreted their results with the aid of optical excitation calculations, which were found to be in good agreement with experiment. Rossouw and Botton also analyzed the resonant modes of bent and kinked silver nanowires for their potential use in nanophotonic circuits.[19] Interestingly, no interruption of the mode propagation was observed due to the bends and kinks, such that the optical response was similar to that of a straight wire.

In this work, we further explore EELS of silver NWs, presenting new data on the detailed dependence of the spectral response on the electron beam position near the nanowire surface. We observe an asymmetrical loss spectrum and spectral shifts in the loss peak that we attribute to high-order mode excitation. To aid interpretation, we compare the experimental results with previously published analytical theories, optical excitation models, and direct calculation of electron energy loss probability.

II. EXPERIMENTAL SETUP

Silver nanowires were synthesized through $CuCl_2$ mediated polyol reduction.[20] 5 ml of ethylene glycol (EG) in a

a)Author to whom correspondence should be addressed. Electronic mail: tnorris@umich.edu

 © 2014 AIP Publishing LLC

20 ml disposable glass vial was submerged in an oil bath and heated to 150 °C under magnetic stirring. After 1 h of heating, 40 ml of 4 mM $CuCl_2{\cdot}2H_2O$ in EG was added and the solution was heated for an additional 15 min. 3 ml of 147 mM polyvinylpyrrolidone (PVP) and 3 ml of 94 mM $AgNO_3$ solutions in EG were synchronously injected into the heated EG solution at a constant flow rate of 0.45 ml/min. Upon the formation of long silver nanowires, an hour from the injection of PVP and $AgNO_3$, the solution turned opaque and wispy gray. The silver nanowires were separated from the EG and PVP by centrifugation at 209 rad/s (2000 RPM) for 20 min in acetone and re-dispersed in water.

The silver nanowires were dispersed in organic solvents by replacing the PVP with an alkanethiol.[21] Specifically, 1 mg/ml of silver nanowires in ethanol were mixed with 10 mM of 1-undecanethiol (UDT) in chloroform in equal volume and sonicated for 10 min after which the mixture was left for 24 h. This allowed for displacement of the PVP and formation of a UDT self-assembled monolayer on the nanowires. The silver nanowires were further purified by centrifugation, supernatant extraction, and re-suspension in target organic solvents.

In preparation for STEM-EELS analysis, silver nanowires were deposited from solution by drop-casting onto a thin lacey-carbon film supported on a standard 3 mm copper mesh grid. EELS spectrum imaging and high-angle annular dark-field imaging (HAADF) were carried out using an FEI Titan 80–300 STEM equipped with a double-hexapole spherical aberration corrector on the probe-forming side of the objective lens and a Wien-filter monochromator.[31] The instrument was operated at an accelerating voltage of 300 kV using an accelerating gun lens resulting in a final probe current of ≈100 pA. While the spherical aberration corrector permits the formation of an electron probe with a diameter of approximately 0.1 nm, additional source magnification is incurred due to the dispersive action of the monochromator. The exact probe shape is difficult to measure and calculate, but the final probe size is on the order of 0.3 nm.

Spectroscopy was carried out with a Gatan Tridiem 865 imaging energy-filter, with typical acquisition times of 100 ms per spectrum, using a convergence angle of 13 mrads and a collection angle of 13 mrads. The energy dispersion was set to 0.01 eV/channel. To provide a measure of the energy-resolution of the system under these conditions, the full-width half maximum and full-width tenth maximum of the zero-loss peak were measured and found to be 0.2 eV and 0.5 eV, respectively. Spectra were aligned in the energy dimension using Matlab code to set the channel with maximum intensity to zero energy-loss. While it was impossible to analyze free-standing NWs, in order to minimize substrate effects, care was taken to analyze only the ends of those NWs that extended far from the underlying amorphous carbon support. STEM-HAADF images were collected both before and after EELS acquisition. Images collected prior to analysis showed that the nanowires exhibited clean surfaces, with no evidence of oxide or carbonaceous surface layers present. However, the presence of ultrathin layers of this kind cannot be entirely ruled out. Images collected after analysis showed that some hydrocarbon deposition did occur during the analysis. No other evidence of specimen alteration was observed.

In order to study the plasmon modes in detail, we performed EELS of individual silver nanowires. In the first set of experiments, we acquired EELS spectra at a series of electron beam positions relative to the nanowire. All spectra are presented as they were acquired, without applying background subtraction or deconvolution. We investigated the dependence of the spectral response on the distance of the beam from the nanowire tip and the distance from the side of the nanowire in a region that was far from the tip. The spectral response was also measured at a fixed distance from the side of the wire as a function of distance from the wire's tip. This measurement was complemented by hyperspectral EELS imaging of the entire region of the nanowire within several hundred nanometers of the tip.

III. RESULTS

EELS spectra collected as a function of beam distance from the tip of the nanowire are shown in Fig. 1(a). The inset shows the experimental setup, where spectra were acquired every nanometer along a 50 nm line (indicated in orange). The acquisition began with the beam positioned inside of the wire and then moving away from it into the surrounding vacuum. A 2-D plot of the spectral response vs. beam position is given in Fig. 1(a), with the white dashed line indicating the interface between the tip of the nanowire and vacuum. A similar set of data was acquired for beam positions scanned perpendicular to the side of the nanowire, and this is shown in Fig. 1(b). Spectra extracted at various intervals along the line of acquisition are presented in Figs. 1(c) and 1(d). In all cases, a strong loss peak due to SPR has been excited near 3.6 eV. The SPR excitation efficiency drops off exponentially as the beam moves away from the wire, corresponding to the confinement of the SPR mode to the metal surface, as has been established by a number of recent studies.[4,18,22,23] When the beam is positioned near the tip of the nanowire, the SPR peak is highly asymmetric and broad. In addition, the peak was observed to continuously shift from ≈3.5 eV when the beam was near the metal-vacuum interface to ≈3.3 eV when the beam was 25 nm away as indicated by the dashed black line in Fig. 1(c). By contrast, as shown in Figs. 1(b) and 1(d), the spectral peak in the transverse case was relatively narrow and was positioned at 3.6 eV regardless of beam position.

SPR propagation along the side of the nanowire was also investigated by positioning the beam at the positions indicated in the STEM image shown in Figure 2(a). The corresponding EELS spectra for each of these positions contain a strong peak at ≈3.6 eV, as well as a series of peaks at lower energy-loss (indicated by arrows). These lower energy-loss peaks are due to the excitation of Fabry-Perot modes along the wire due to its finite length.[17,18] Moreover, it is shown that the strongest silver SPR peak occurs at ≈3.6 eV when the beam is positioned along the side of the wire, but that the peak shifts to ≈3.5 eV when the beam is moved to the tip of the nanowire. This observed difference in the energy-loss position is consistent with the previously presented spectra.

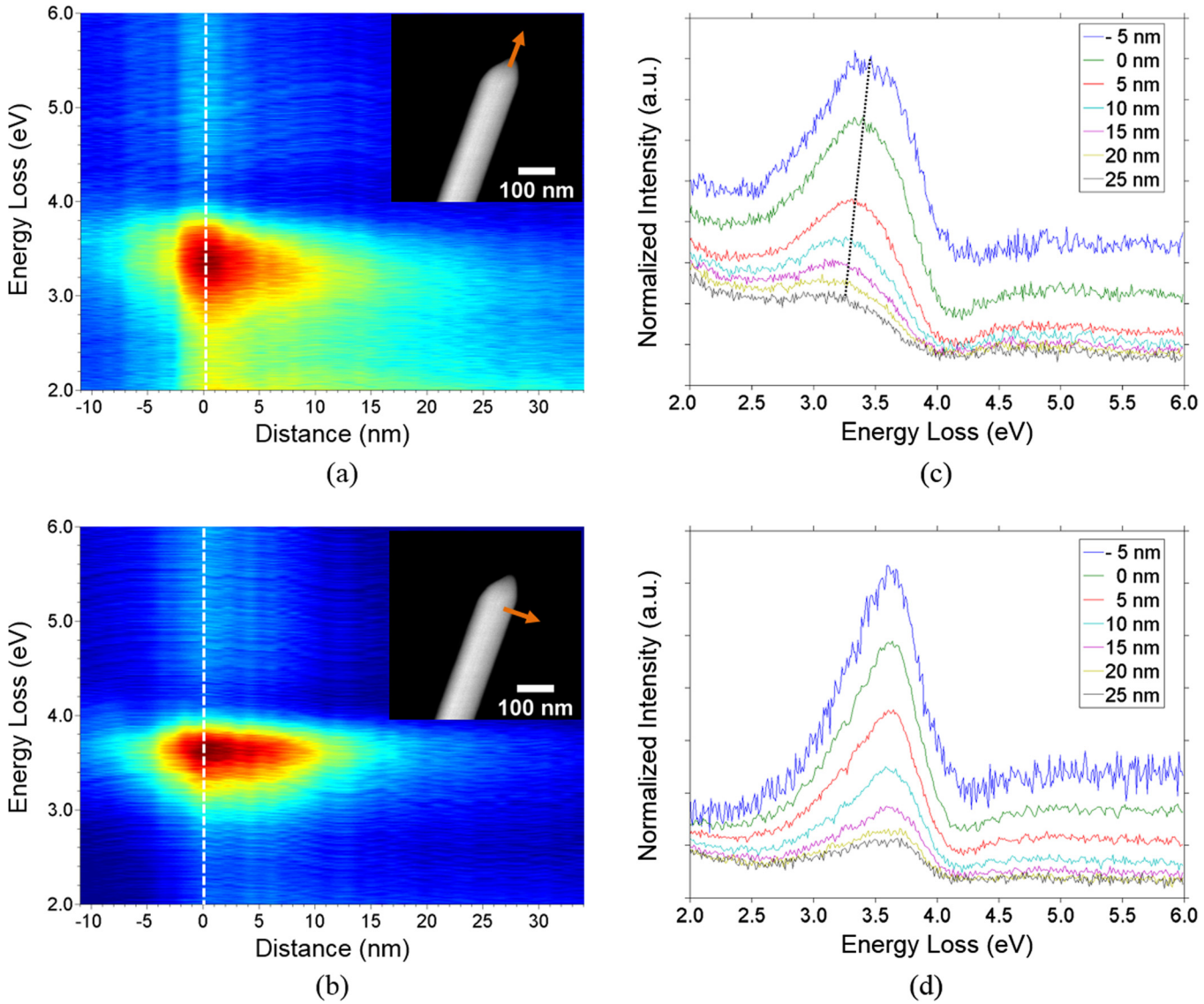

FIG. 1. Experimental EELS spectra collected near the end of a 100 nm diameter silver nanowire with the beam traveling in (a) the longitudinal direction and (b) the transverse direction. The inset STEM-HAADF images show the region analyzed. Data were collected serially in 1 nm increments in the direction indicated by the orange arrow. The white dashed line overlaid in the EELS data represents the interface between the silver nanowire and vacuum which is set as the origin of the abscissa. Also shown are EELS spectra as a function of distance from the nanowire surface along the (c) longitudinal direction and (d) the transverse direction.

Figs. 2(b) and 2(c) show another STEM-HAADF image of the nanowire and the corresponding spectra obtained along the wire surface at the indicated positions. In this case, the Fabry-Perot modes are again observed at low energy-loss in addition to a pair of stronger peaks positioned at 3.5 eV and 3.75 eV. As discussed previously, the former peak is due to the delocalized SPR at the wire-vacuum boundary, while the latter is due to the bulk plasmon loss as the beam passes through the wire itself.[4,24,25]

The spatial distribution of the low-energy modes was observed by extracting images from an EELS spectrum image at varying energy-loss values, and a subset of the data is shown in Fig. 3(a). As observed in the previous studies,[17–19] the propagating modes along the length of the wire become standing waves in a finite system due to boundary confinement resulting in the Fabry-Perot type resonances. These images can be compared to simulated electric field distributions obtained by finite-difference time-domain (FDTD) simulations of the optical response of the nanowire (Fig. 3(b)) and the results are qualitatively quite similar. By measuring the spatial separation between the peaks of each SPR mode in Figs. 3(a) and 3(b), the dispersion relations are obtained and plotted in Fig. 3(c). The values of k (in nm^{-1}) are measured from the experimental EELS series in Fig. 3(a) and the simulated series in Fig. 3(b). k is given by

$$k = \frac{2\pi}{\lambda_{sp}},$$

where λ_{sp} is the wavelength between two resonance peaks. For a given resonance mode, the spacing between adjacent maxima of intensity varies slightly along the silver nanowire, so that the k does not have a unique value. The theoretical dispersions from a model neglecting retardation and substrate

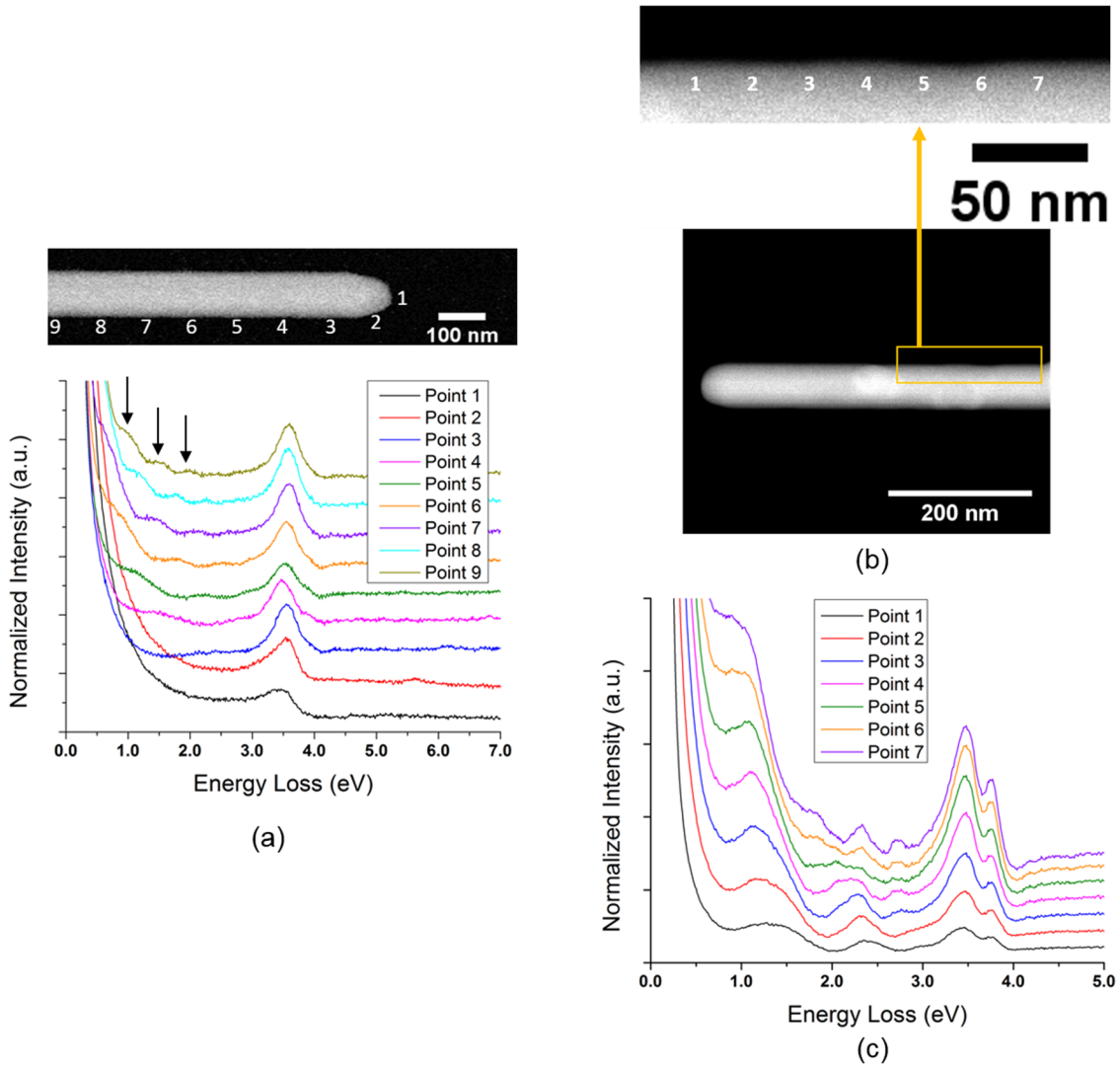

FIG. 2. (a) STEM-HAADF image of 100 nm diameter silver nanowire and corresponding EELS spectra extracted from the numbered locations. The strongest SPR peaks are at ≈3.5 eV to ≈3.6 eV, while the black arrows highlight the Fabry-Perot resonances observed at lower energy-loss, the position of which depends strongly on distance from the nanowire tip. (b) STEM-HAADF image of a silver nanowire and a zoomed image of the region analyzed by EELS. (c) Corresponding EELS spectra extracted from the seven numbered positions denoted in (c).

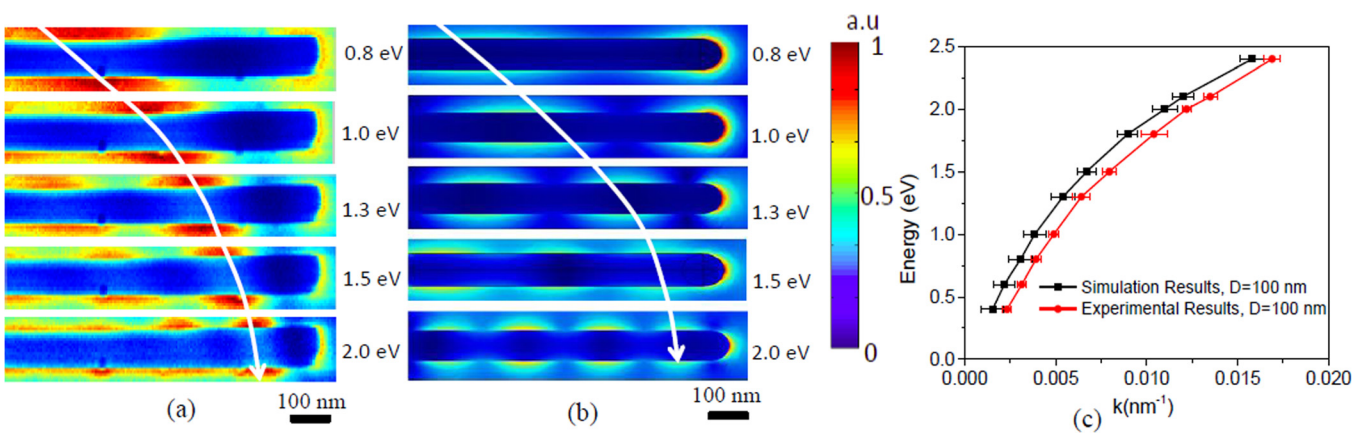

FIG. 3. (a) Images extracted from a EELS hyperspectral dataset acquired from near the end of a 100 nm diameter. The images show the spatially resolved EELS response at various energy-loss values and depict the standing wave pattern in the nanowire resulting from surface plasmon resonances. (b) Simulated electric field distributions resulting from optical excitation of a model silver nanowire. The intensity has been scaled independently for all of the images in. (c) Experimental and calculated dispersion relations as a function of wavenumber k, where $k = 2\pi/\lambda sp$ and $\lambda sp/2$ is the half wavelength measured between two resonance peaks. Note that the k values are not uniquely defined but have an error range, as the EELS signal is not perfectly periodic.

effects are also shown; clearly, a small systematic shift is observed between the model and experimental dispersions, which may be due to limiting assumptions of the model as well as effects due to shape, size, and composition.[19]

IV. DISCUSSION

To investigate the features observed in the collected spectra and the relation between the optical and energy loss responses, we first performed EELS simulations using the MNPBEM toolbox.[26] The nanowire was modeled as a 1 μm long cylindrical wire with spherical caps at both ends; the wire diameter was set to 100 nm. Values for the silver permittivity were extracted from optical experiments,[27] and the EELS maps and spectra were computed according to the protocol given previously.[28,29]

In Figure 4, the calculated EELS response is shown as a function of distance from the nanowire when the beam is moving in the longitudinal and transverse directions (Figs. 4(a) and 4(b), respectively). The interface between the nanowire and vacuum is again denoted by the white dashed lines. The corresponding spectra for selected impact parameters are also shown in Figs. 4(c) and 4(d). In both cases, a number of peaks associated with Fabry-Perot resonances are observed at lower loss energies (<3 eV), which then merge into a continuum of states around 3.60 eV. Also, in both sets of simulations, a peak is observed at 3.75 eV when the beam is positioned inside the nanowire, which corresponds to excitation of the bulk plasmon for silver. If only the asymptotic SPR peak near 3.60 eV is considered, a higher degree of dispersion was observed in the longitudinal case than in the transversal. This can be seen in the insets of Figs. 4(c) and 4(b), which enlarge this spectral region near the wire surface, as well as in Fig. 4(c) where the peak near 3.6 eV shifts to lower energies when the electron beam moves away from the nanowire. In contrast, the asymptotic peak in the inset of Fig. 4(b) and in Fig. 4(d) shows almost no dispersion whatsoever. Therefore, the experimental and theoretical results show very nice agreement, especially in the asymptotic regime.

However, there are some interesting differences between the acquired spectra and the calculated EELS response. First, in the experimental EELS data, the Fabry-Perot modes are much less distinct than the EELS calculations suggest. This is likely due to the finite energy resolution of the experimental data. Indeed, when the simulated spectra are convolved

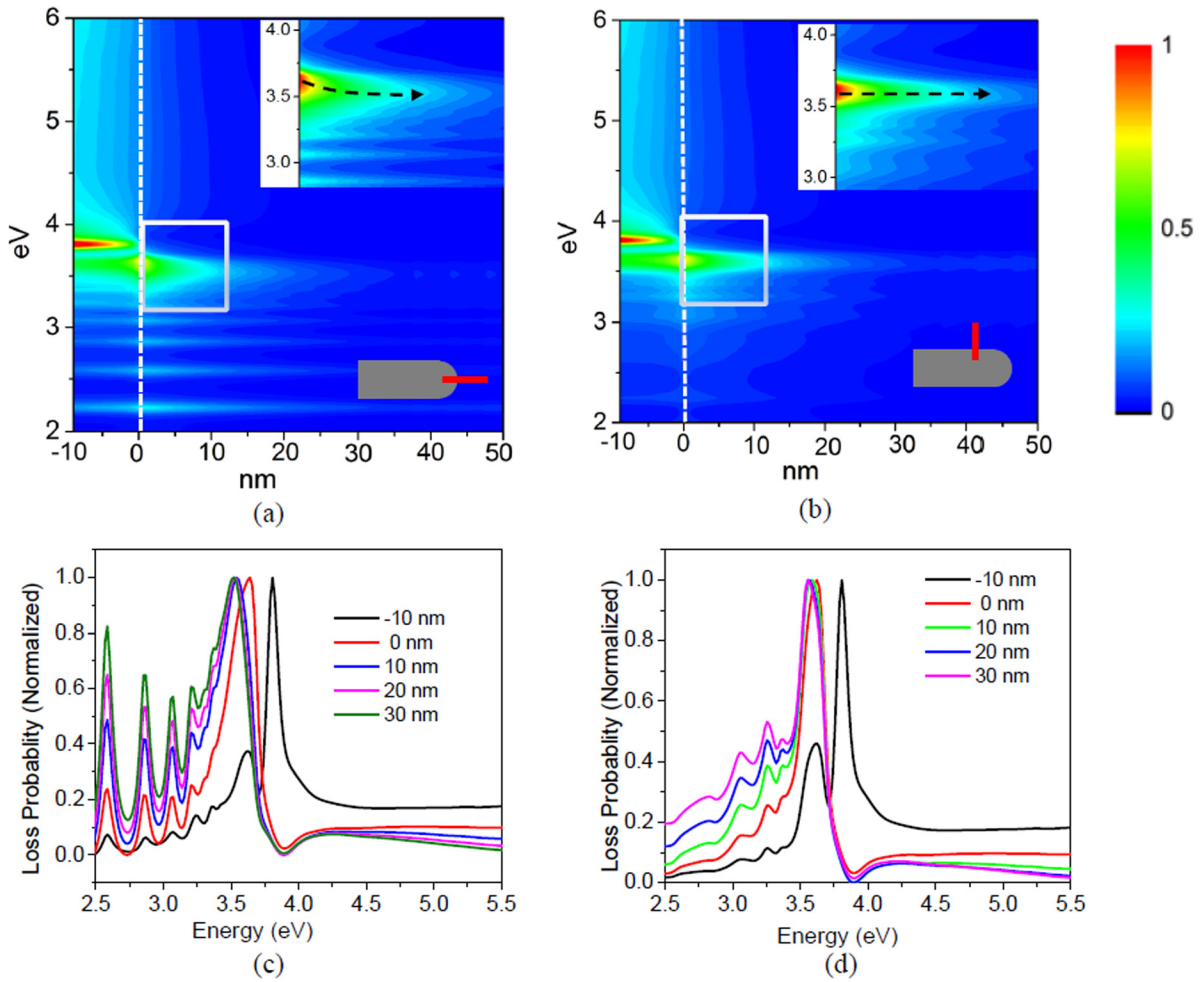

FIG. 4. Simulation results for a cylindrical nanowire of 1 μm length and 100 nm diameter, using the MNPBEM toolbox.[27] Density plot for electron energy loss maps as a function of loss energy and impact parameter along the (a) longitudinal and (b) transversal directions. The insets show a magnified view of the asymptotic regime, marked by the white box. The nanowire boundary at 0 nm is shown by the dashed line. (c) and (d) Corresponding spectra for selected impact parameters.

with a Gaussian function with FWHM = 0.3 eV (shown in Fig. 5), the pronounced peak structure is almost completely indiscernible and the simulated spectra more closely match those acquired experimentally (Figs. 1(b) and 1(d)) quite well. Therefore, the modeled spectra indicate that the origin of the observed spectral asymmetry arises from the contributions of the high-k longitudinal modes on the low energy side of the SPR peak. Another discrepancy is that the bulk peak is less intense in the experimental data and optical excitation calculation than in the EELS simulations. A quantitative explanation of this requires further work but is possible that this effect is due to the attenuation of the electron beam within the metal nanowire, which is not accounted for in the EELS calculations.

While the EELS spectra calculated using the MNPBEM toolbox nicely replicated the spectral shift behavior observed in our experiments, they did not indicate what the origin of this behavior could be. In order to obtain physical insight into the observed plasmonic modes and the relation between the nanoscale optical and EELS responses, we then carried out detailed simulations using energy loss theories and optical models. A theoretical description of the collective electronic excitations at metal surfaces has been presented by Pitarke *et al.*,[25] who predicted that a number of multipolar modes can be excited and contribute to the energy loss of moving electrons. To approximate the nanowires that were examined experimentally, we have considered two distinct geometries. First, a semi-spherical model was used to approximate the tip of the nanowire, although it is apparent from the image in Fig. 1 that the true tip geometry deviates from this simplified geometry. To compare the analytical theory of energy loss with the optical response of this silver nanosphere, we performed numerical simulations using the FDTD Lumerical package, assuming excitation by an optical dipole source at different positions to mimic the electron beam positions. The frequency dependent dielectric function of silver was taken from previously reported optical data.[30]

Figure 6(a) presents a schematic of the silver nanosphere model used to approximate the nanowire tip. The red line in Fig. 6(a) depicts the electron beam traveling at a particular distance, b, from the center of the silver nanosphere. Fig. 6(b) shows the calculated FDTD normalized power flow distribution as a function of distance from a silver nanosphere with diameter of 100 nm. The origin of the x-axis is set in the nanosphere, and the white dashed line at x = 0 denotes the interface between the sphere's surface and vacuum. When the beam is positioned within the sphere, the resonance peak is observed at ≈3.7 eV, which corresponds to the bulk plasmon energy. This peak is stable as the beam moves towards the surface of the sphere. However, when it reaches the interface and progresses away from the sphere, the resonance peak steadily shifts towards ≈3.5 eV. The inset in Fig. 6(b) presents the electric field power flow distribution in the region near the nanowire tip. The black dashed curve with arrow indicates the resonance peak position as the beam moves away from the tip. The spectral shift observed in this simulation agrees quite well with that observed in the experimental EELS data (Figs. 1(a) and 1(c)).

To investigate the origin of this shift, the electron energy-loss probability was also calculated analytically for the spherical model.[25] Fig. 6(c) shows the results of this calculation for several SPR resonance modes: the dipole mode (mode index $\ell = 1$), quadrupole mode ($\ell = 2$), octupole mode ($\ell = 4$), and hexadecapole mode ($\ell = 8$). In this case, the resonance peaks are seen to shift from 3.50 eV for $\ell = 1$ to 3.66 eV for $\ell = 8$. In addition, the higher order modes are noticeably more localized at the surface of the sphere than the lower order modes which extend much further into vacuum. Since the tip of the nanowire analyzed using EELS can be considered pseudo-spherical, these analytical computations suggest that the spectral shift observed in the experimental data (Figs. 1(a) and 1(c)) arises due to the differences in energy-loss probabilities between the lower- and higher-order modes. When the beam is positioned near the nanowire surface, the more localized, higher-order modes contribute more significantly. As the beam moves away from the surface, the energy-loss is

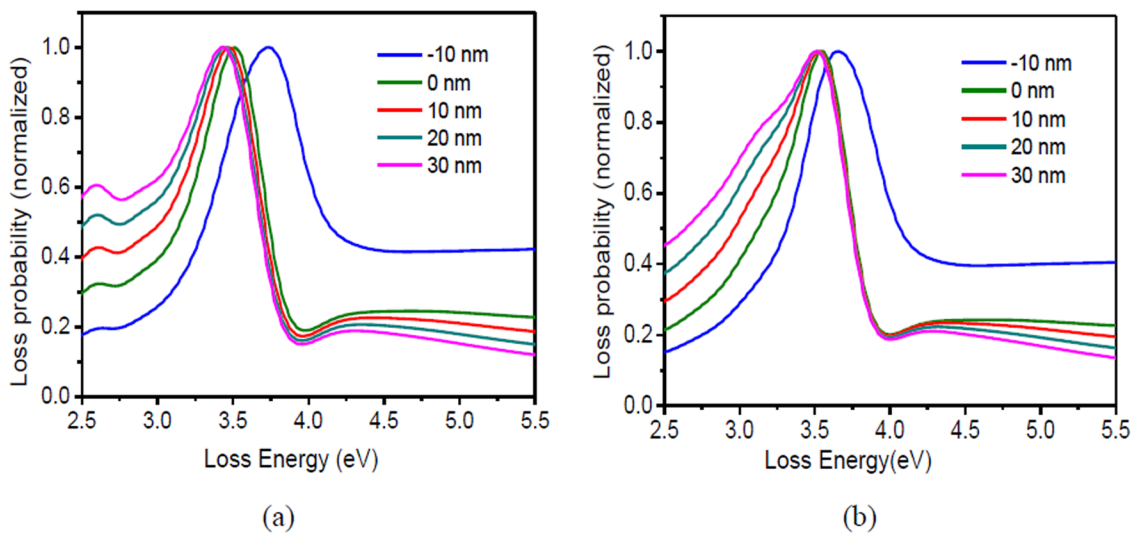

FIG. 5. Simulated spectra from the (a) longitudinal and (b) transversal directions after convolution with a Gaussian function (FWHM = 0.3 eV).

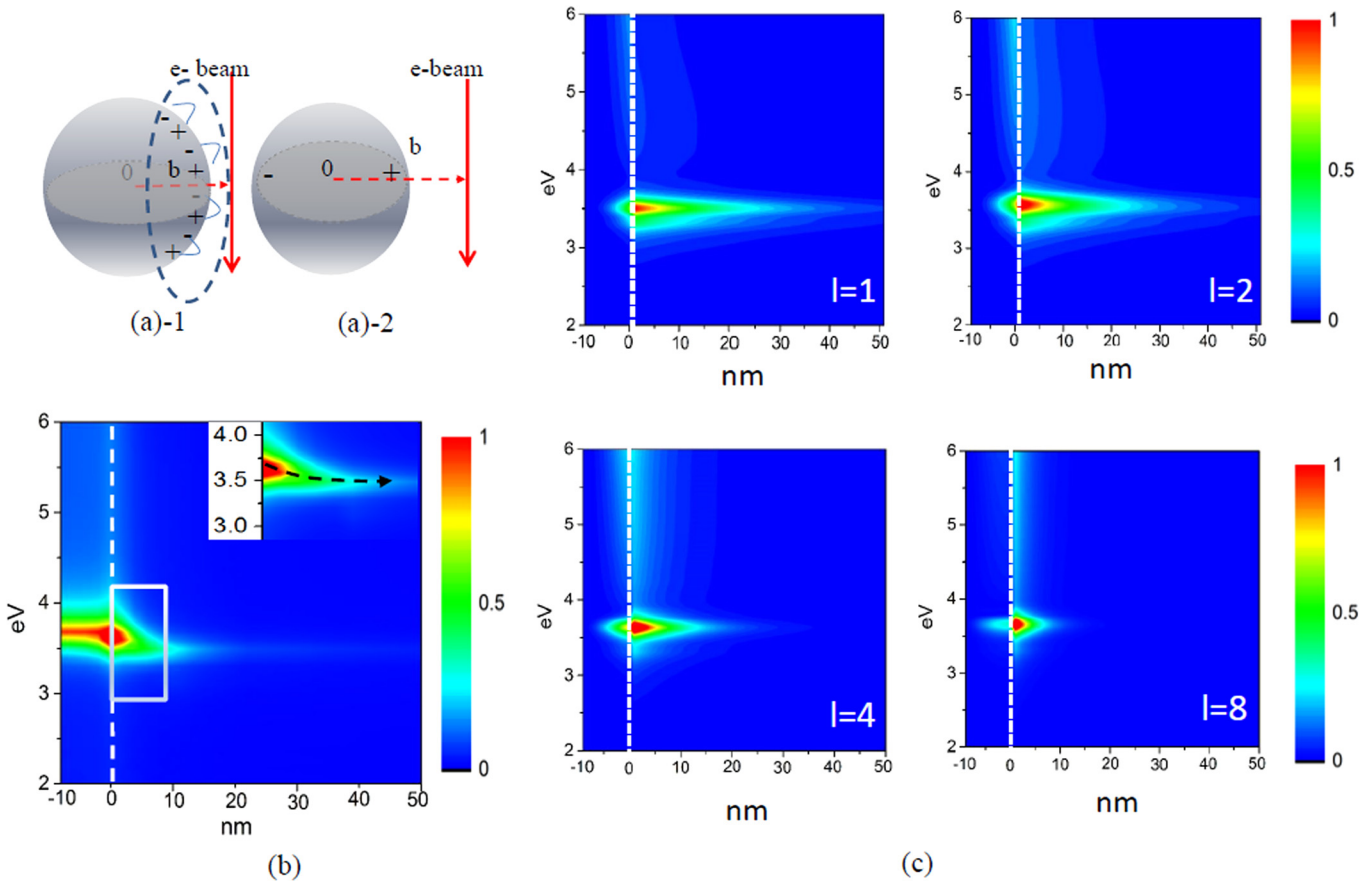

FIG. 6. Results of analytical energy loss and optical simulations for an ideal silver nanosphere. (a) Schematics of the surface charge densities induced by an electron beam (denoted by the red line) placed (a-1) close to the surface of the sphere and (a-2) far away from the surface of the sphere. (b) FDTD simulated power flow intensity distributions as a function of distance from the surface of an ideal silver nanosphere under optical excitation. The position of the surface is indicated by the white dashed line at 0 nm. (c) Analytically computed electron energy loss probabilities from the silver nanosphere for various resonance modes (mode index $\ell = 1$, 2, 4, and 8). Due to the strong variation in maximum energy-loss intensity and for better visibility, the color scale has been scaled independently for all of the images.

dominated by the more delocalized dipole mode resulting in a shift of the observed resonance peak to lower energy-loss. As discussed by Pitarke *et al.*[25] and shown schematically in Fig. 6(a-1), multipolar resonances are readily excited when the beam is near the edge of the sphere since it effectively interacts with a nearly planar surface. In contrast, the dipole resonance will be dominant when the beam is far from the surface of the nanosphere and the impact parameter is large (Fig. 6(b-2)).

To model the EELS response when the beam was positioned along the side of the nanowire, we have performed similar calculations using an infinitely long cylinder geometry.[25] Figure 7(a) shows a schematic of this case where the solid red line represents the electron beam trajectory and the dashed red line indicates its distance, b, from the center of the cylinder. Fig. 7(b) shows the FDTD calculated normalized power flow distribution as a function of radial distance. In contrast to the case of the spherical model, in this case, the power flow shows a single peak at ≈3.6 eV that does not shift as the beam moves away from the cylinder. The inset in Fig. 7(b) depicts the power flow distribution from the region near the edge of the cylinder, and the dashed black line shows a consistent resonance peak that does not shift with excitation position. The observed insensitivity of the peak energy-loss with beam position differs markedly from the calculations for the spherical model but agrees quite well with the experimental EELS data.

Once again, to investigate the origin of these observations, the analytical energy loss probabilities for the various modes ($\ell = 1$–8) were calculated, and the results are presented in Figure 7(c). For all four modes, peaks are observed at ≈3.65 eV and ≈3.3 eV, which are confined near the interface region. For the dipole mode ($\ell = 1$) ,these two peaks exhibit very similar amplitudes. However, as ℓ increases, the higher energy-loss peak becomes progressively more intense relative to the lower energy-loss peak. These results fit quite well with the peak shapes and intensities observed in the experimental EELS spectra collected along the side of the nanowire (Figs. 1(d) and 2(c)), suggesting that the multipolar resonances dominate the SPR response in this case. Finally, despite the differences in amplitude, the peak positions for all four modes do not change as a function of distance from the nanowire surface. This is markedly different from the calculations already discussed for the spherical model but matches the behavior observed in the experimental EELS spectra acquired in the transverse orientation. Therefore, the characteristics of the SPR peak in the two experimental cases we have investigated can be explained by the spatial dependence of the energy-loss probabilities of the various modes excited by the electron beam.

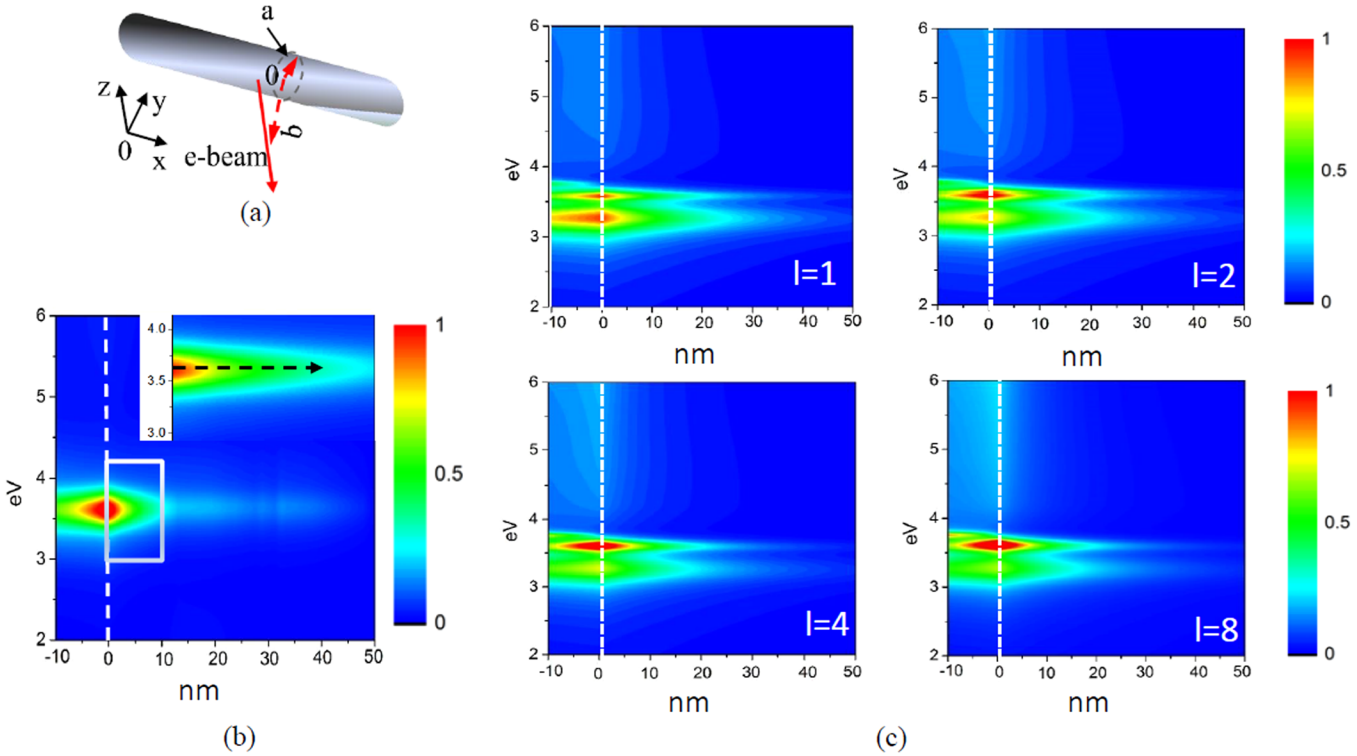

FIG. 7. Results of analytical energy loss and optical simulations for an ideal 100 nm diameter silver nanocylinder. (a) Schematic showing the 100 nm diameter cylinder lying in the (x,y) plane with the electron beam (solid red line) positioned parallel to the z-axis. The dashed red line indicates the distance from the beam to the center of the cylinder. (b) FDTD simulated power flow intensity distributions as a function of distance from surface of the silver nanocylinder under optical excitation. The cylinder surface is indicated by the white dashed line at 0 nm. (c) Analytically computed electron energy loss probabilities from the silver nanocylinder for various resonance modes (mode index $\ell = 1$, 2, 4, and 8). Due to the strong variation in maximum energy-loss intensity and for better visibility, the color scale has been scaled independently for all of the images.

V. CONCLUSIONS

We have explored the detailed spatial dependence of the electron energy loss at optical frequencies when the electron beam is directed near the surface of silver nanowires. Due to the pseudospherical shape of nanowire tip, the detailed loss spectrum near this region depends strongly on the position of the electron beam. Far from the tip, the spectral response is dominated by the dipolar excitation, as predicted theoretically for a spherical geometry. As the beam approaches the tip, the surface of the wire becomes effectively planar, resulting in the excitation of higher-order modes and a shift of the resonance peak towards higher energies. The spectral response was simulated in three ways: (1) using previously published analytical models of energy loss for ideal spheres and infinite wires, (2) by calculating the optical response with dipole optical field excitation, and (3) by simulating the EELS maps using a boundary element method. With the aid of these calculations, it was shown that the spatial variations of the loss peak in the experimental spectra were due to excitation of the more localized higher-order modes when the beam is very close to the nanowire surface. For detailed calculation of the loss spectra and the spatial response profiles, both numerical optical excitation and energy loss simulations showed good agreement with the experimental results. These experiments and calculations demonstrate that the energy loss and optical spectra provide complementary insight into the plasmonic modes of metallic nanostructures.

ACKNOWLEDGMENTS

This work was supported by the Center for Photonic and Multiscale Nanomaterials (C-PHOM) funded by the National Science Foundation Materials Research Science and Engineering Center program DMR 1120923.

This material is also based upon work partially supported by the Center for Solar and Thermal Energy Conversion, an Energy Frontier Research Center funded by the U.S. Department of Energy, Office of Science, Office of Basic Energy Sciences under Award No. #DE-SC0000957 used to purchase materials for NP and nanowire synthesis.

The portion of the work at Karl-Franzens-Universität Graz has been supported by the Austrian Science Fund FWF under Project P24511-N26 and the SFB NextLite.

[1]Y. G. Sun and Y. N. Xia, Science **298**(5601), 2176–2179 (2002).
[2]I. Washio, Y. J. Xiong, Y. D. Yin, and Y. N. Xia, Adv. Mater. **18**(13), 1745–1749 (2006).
[3]T. K. Sau and C. J. Murphy, Langmuir **20**, 6414 (2004).
[4]M. N'Gom, J. Ringnalda, J. F. Mansfield, A. Agarwal, N. Kotov, N. J. Zaluzec, and T. B. Norris, Nano Lett. **8**, 3200 (2008).
[5]M. N'Gom, T. B. Norris, and R. Erni, in *Conference on Lasers and Electro-Optics and 2009 Conference on Quantum Electronics and Laser Science Conference, Baltimore, MD, USA, 31 May–5 June 2009* (IEEE, New York, 2009), pp. 3228–3229.
[6]L. Novotny, Phys. Rev. Lett. **98**, 266802 (2007).
[7]E. R. Encina, E. A. Perassi, and E. A. Coronado, J. Phys. Chem. A **113**, 4489 (2009).
[8]E. J. R. Vesseur, R. de Waele, M. Kuttge, and A. Polman, Nano Lett. **7**, 2843 (2007).

[9]F. J. Garcia de Abajo and M. Kociak, Phys. Rev. Lett. **100**, 106804 (2008).
[10]J. Nelayah, M. Kociak, O. Stephan, F. J. G. de Abajo, M. Tence, L. Henrard, D. Taverna, I. Pastoriza-Santos, L. M. Liz-Marzan, and C. Colliex, Nat. Phys. **3**, 348 (2007).
[11]P. E. Batson, N. Dellby, and O. L. Krivanek, Nature **418**, 617 (2002).
[12]P. M. Echenique and J. B. Pendry, J. Phys. C: Solid State Phys. **11**, 2065 (1978).
[13]M. V. Bashevoy, F. Jonsson, A. V. Krasavin, N. I. Zheludev, Y. Chen, and M. I. Stockman, Nano Lett. **6**, 1113 (2006).
[14]R. H. Ritchie, Surf. Sci. **34**, 1 (1973).
[15]M. Rocca, Surf. Sci. Rep. **22**, 1 (1995).
[16]T. L. Ferrell and P. M. Echenique, Phys. Rev. Lett. **55**, 1526 (1985).
[17]O. Nicoletti, M. Wubs, N. A. Mortensen, W. Sigle, P. A. van Aken, and P. A. Midgley, Opt. Express **19**, 15371 (2011).
[18]D. Rossouw, M. Couillard, J. Vickery, E. Kumacheva, and G. A. Botton, Nano Lett. **11**, 1499 (2011).
[19]D. Rossouw and G. A. Botton, Phys. Rev. Lett. **110**, 066801 (2013).
[20]K. E. Korte, S. E. Skrabalak, and Y. N. Xia, J. Mater. Chem. **18**, 437 (2008).
[21]P. Andrew and A. Ilie, J. Phys.: Conf. Ser. **61**, 36 (2007).
[22]C. J. Rossouw, L. J. Allen, S. D. Findlay, and M. P. Oxley, Ultramicroscopy **96**, 299 (2003).
[23]A. L. Koh, D. W. McComb, S. A. Maier, H. Y. Low, and J. K. W. Yang, J. Vac. Sci. Technol., B **28**, C6O45 (2010).
[24]R. H. Ritchie, Phys. Rev. **106**, 874 (1957).
[25]J. M. Pitarke, V. M. Silkin, E. V. Chulkov, and P. M. Echenique, Rep. Prog. Phys. **70**, 1 (2007).
[26]U. Hohenester and A. Trugler, Comput. Phys. Commun. **183**, 370 (2012).
[27]E. D. Palik, *Handbook of Optical Constants of Solids* (Academic, Orlando, 1985).
[28]U. Hohenester, Comput. Phys. Commun. **185**, 1177 (2014).
[29]F. J. Garcia de Abajo, Rev. Mod. Phys. **82**, 209 (2010).
[30]P. B. Johnson and R. W. Christy, Phys. Rev. B **6**, 4370 (1972).
[31]Commercial equipment, instruments, and materials or software is identified in this report to specify adequately the experimental procedure. Such identification does not imply recommendation or endorsement of these items by the NIST nor does it imply that they are the best available for the purpose.